The Astrophysical Journal Letters, 732:L26 (6pp), 2011 May 10 doi:10.1088/2041-8205/732/2/L26

FAST COALESCENCE OF MASSIVE BLACK HOLE BINARIES FROM MERGERS OF GALACTIC NUCLEI: IMPLICATIONS FOR LOW-FREQUENCY GRAVITATIONAL-WAVE ASTROPHYSICS

Miguel Preto[1,2], Ingo Berentzen[1,3], Peter Berczik[1,4,5], and Rainer Spurzem[1,4,6]
[1] Astronomisches Rechen-Institut, Zentrum für Astronomie, University of Heidelberg, D-69120 Heidelberg, Germany
[2] Max Planck Institut für Gravitationsphysik (Albert-Einstein-Institut), D-14476 Potsdam, Germany
[3] Institut für Theoretische Astrophysik, Zentrum für Astronomie der University of Heidelberg, Albert-Ueberle-Str. 2, D-69120 Heidelberg, Germany
[4] National Astronomical Observatories of China, Chinese Academy of Sciences NAOC/CAS, 20 A Datun Rd., Chaoyang District, Beijing 100012, China
[5] Main Astronomical Observatory (MAO), National Academy of Sciences of Ukraine (NASU), Akademika Zabolotnoho 27, 03680 Kyiv, Ukraine
[6] The Kavli Institute for Astronomy and Astrophysics, Peking University, Beijing, China
Received 2011 February 23; accepted 2011 March 29; published 2011 April 15

ABSTRACT

We investigate a purely stellar dynamical solution to the Final Parsec Problem. Galactic nuclei resulting from major mergers are not spherical, but show some degree of triaxiality. With *N*-body simulations, we show that *equal-mass* massive black hole binaries (MBHBs) hosted by them will continuously interact with stars on centrophilic orbits and will thus inspiral—in much less than a Hubble time—down to separations at which gravitational-wave (GW) emission is strong enough to drive them to coalescence. Such coalescences will be important sources of GWs for future space-borne detectors such as the *Laser Interferometer Space Antenna* (*LISA*). Based on our results for equal-mass mergers, and given that the hardening rate of unequal-mass binaries is similar, we expect that *LISA* will see between $\sim$10 and $\sim$ few $\times\ 10^2$ such events every year, depending on the particular massive black hole (MBH) seed model as obtained in recent studies of merger trees of galaxy and MBH co-evolution. Orbital eccentricities in the *LISA* band will be clearly distinguishable from zero with $e \gtrsim 0.001$–0.01.

Key words: black hole physics – galaxies: nuclei – gravitational waves

1. INTRODUCTION

Massive black hole binaries (MBHBs) are one of the most interesting sources of gravitational waves (GWs) for future space-borne detectors such as the *Laser Interferometer Space Antenna* (*LISA*). They are expected to coalesce under the strong emission of GWs, after stellar- and/or gas-dynamical processes bring them to separations small enough ($a_{\rm GW} \sim 10^{-3}$ pc) that GW emission is efficient in making them coalesce in less than a Hubble time (Milosavljević & Merritt 2003; Armitage & Natarajan 2005). It is still an open problem whether prompt MBHB coalescences are generic, or whether long-lived binaries are the norm.

The paradigm for MBH binary evolution, after a merger of gas-poor galaxies, consists of three distinct phases (Begelman et al. 1980). First, the two massive black holes (MBHs) sink toward the center due to the dynamical friction exerted by the stars. This process continues after they form a bound pair with semimajor axis $a \sim r_h$, where r_h is the binary's influence radius defined to be the radius that encloses twice the mass of the binary in stars. It stops when the binary reaches the *hard binary* separation $a \sim a_h$ (Yu 2002):

$$a_h := \frac{G\mu_r}{4\sigma^2} \sim \frac{1}{4}\frac{q}{(1+q)^2} r_h, \qquad (1)$$

where μ_r is the binary's reduced mass, σ is the one-dimensional velocity dispersion, $q = M_{\bullet,2}/M_{\bullet,1}$ is the binary's mass ratio. Second, for $a \lesssim a_h$, as dynamical friction becomes inefficient in further driving the inspiral, it is instead the *slingshot* ejection of stars that dominates. Third, the binary eventually reaches a separation $a_{\rm GW}$ at which the loss of orbital energy to GW emission drives the final coalescence. The transition from the first to the second phase is prompt provided that the mass ratio of the remnants is not too small, $q = M_2/M_1 \gtrsim 0.1$ (Colpi & Dotti 2009). In contrast, the subsequent transition from the second to the third phase could constitute a bottleneck for the binary evolution toward final coalescence. This is the so-called Final Parsec Problem.

In *quasi-steady spherical* stellar environments, the binary's hardening rate $s(t) \equiv d/dt(1/a)$ slows down significantly once it reaches separations a few times below $\sim a_h$ (Quinlan & Hernquist 1997; Milosavljević & Merritt 2003; Berczik et al. 2005). In these spherical and gas-poor nuclei, two-body relaxation is the only mechanism for populating the binary's loss cone,[7] but being a slow diffusive process, it is only in low-luminosity galaxies harboring MBHs of mass $M_\bullet \lesssim$ few $\times\ 10^6\ M_\odot$ that central relaxation times are short enough to drive the binary to coalescence (Yu 2002; Merritt et al. 2007).

But spherical models are a *worst case scenario*. Merger remnants will generally be irregular with some degree of triaxiality and, even if triaxiality would only be a rather mild and transient phenomenon, it may suffice to bring the binary down to $a_{\rm GW}$ (Yu 2002; Merritt & Poon 2004). Berczik et al. (2006) and Berentzen et al. (2009) studied triaxial, rotating models of galactic nuclei using *N*-body simulations. They have shown that MBHBs in such models coalesce in much less than a Hubble time. The next logical step is to study mergers of galactic nuclei to investigate whether the latter results still hold true under more realistic models and initial conditions.

In this Letter, we use *N*-body simulations to show that: (1) in merging nuclei, the hardening rate is *N*-independent—allowing the extrapolation of *N*-body results to real galaxies; (2) the triaxiality depends on the orbital parameters of the progenitor galaxies: prolate shapes occur when the merger is almost radial, while an oblate morphology is the result of a less radial merger; (3) MBHs become bound with high eccentricities

[7] The loss cone is the region of phase space corresponding to orbits that cross the binary, i.e. with angular momentum $J \lesssim J_{\rm lc} = \sqrt{GM_{12} f a_{\rm bin}}$, $f = \mathcal{O}(1)$ (Lightman & Shapiro 1977).

Table 1
N-body Integrations

$M_{12}\backslash N$	64K	128K	256K	512K	1M
0.005	$\lambda_{\rm sph}$	$\lambda_{\rm sph}$	$\lambda_{\rm sph}$	$\lambda_{\rm sph}$	$\lambda_{\rm sph}$
0.1	$\lambda_{\rm sph}$	$\lambda_{\rm sph}$	$\lambda_{\rm sph}$	$\lambda_{\rm sph}$	···
0.005	λ_2	λ_2	λ_2	λ_2	λ_2
0.01	λ_1, λ_2	λ_1, λ_2	λ_1, λ_2	λ_1, λ_2	···
0.02	λ_1, λ_2	λ_1, λ_2	λ_1, λ_2	λ_1, λ_2	···
0.1	λ_1, λ_2	λ_1, λ_2	λ_1, λ_2	λ_1, λ_2	···

Notes. First column: mass of the MBH binary; other columns: particle number *N*; first two lines: simulations of spherical nuclei; last four lines: simulations of merging nuclei; $\lambda = L/L_c$ measures the initial orbital angular momentum of the MBH binary ($\lambda_{\rm sph} = 0.5$ for spherical nuclei), or otherwise it measures the initial orbital angular momentum of the merging nuclei ($\lambda_1 = 0.14$ for near-radial merger and $\lambda_2 = 0.6$ for less radial merger). All nuclei have $\gamma = 1$; all binaries have equal mass $q = M_{\bullet,2}/M_{\bullet,1} = 1$.

(up to $e \sim 0.95$); (4) the eccentricity tends, on average, to increase, in good agreement—often quantitative—with the Quinlan (1996) predictions; (5) high eccentricities assist the MBHB into promptly coalescencing in much less than a Hubble time; and (6) eccentricities in the *LISA* band are likely to be distinguishable from zero ($e \gtrsim 0.001$–0.01) even though GW circularizes the orbits, and will also be quite large ($0.4 \lesssim e \lesssim 0.8$) in the Pulsar Timing Array (PTA) band. While we were finishing the write-up of this Letter, we have learned of another paper with similar results regarding the *N*-independence (Khan et al. 2011).

2. MODELS AND INITIAL CONDITIONS

We have performed two sets of *N*-body experiments. In both, galactic nuclei are represented by spherically symmetric models (Dehnen 1993; Tremaine et al. 1994). These models have a central power-law density profile, $\rho(r) = (3-\gamma)M_T r_b/4\pi r^\gamma (r_b + r)^{4-\gamma}$, with logarithmic slope γ. The total mass of each nucleus is set $M_T = 1$; we adopt units where $G = r_b = 1$. The total mass of the binary is $M_{12} = M_{\bullet,1} + M_{\bullet,2}$, we take $q = 1$.

The set (A) consists of a single spherical nucleus where two MBHs are placed symmetrically about the center, on an unbound orbit, with initial separation $\Delta r_0 = 2$, initial angular momentum $L/L_c = 0.5$, where L_c is the angular momentum of the local circular orbit. The set (B) consists on the merger of two initially bound—but well-separated—spherical nuclei, each of which has a single MBH at the center with zero initial velocity with respect to its nucleus. For B, the initial separation Δr_0 refers to both nuclei taken as if they were point masses. The half-mass radius of each nucleus is $r_{1/2} \approx 2.41$; accordingly, in order to initially have well-separated nuclei, while minimizing the computing time, we set $\Delta r_0 = 20$. For the initial orbital angular momentum of the binary nuclei, we have taken two values $L/L_c = 0.14$ and 0.6 given the nearly parabolic encounters typical of major galaxy mergers from cosmological simulations (Khochfar & Burkert 2006). During the first pericenter passages, the MBH separations are $\Delta r_{\rm BH} \sim 0.2 \sim 0.1 r_{1/2}$ and $\Delta r_{\rm BH} \sim 2.2 \sim r_{1/2}$, respectively. Table 1 lists the runs and adopted parameters.

We have performed the *N*-body simulations using the parallel φ-GPU code. This is an unpublished variant of the parallel direct *N*-body code φ-GRAPE (Harfst et al. 2007), which uses GPU accelerator cards on parallel clusters. It includes a fourth-order Hermite integration scheme, with block time steps, analogous to NBODY1 (Aarseth 2003). The softening length has to be chosen small enough that it reproduces the refilling of the binary's loss cone by two-body relaxation. We adopt a softening length $\epsilon = 10^{-4}$. We set the time step parameter to $\eta_* = 0.01$ for the stars and $\eta_{\rm BH} = 0.001$ for the black holes (BHs). We force the MBHs to be advanced synchronously at all times with the smallest step.

3. MBH EVOLUTION IN SPHERICAL VERSUS IN MERGING NUCLEI

The stars driving the orbital decay of a hard MBHB are those that enter the loss cone orbits. The MBHB's hardening rate is thus determined by the product of the flux of stars entering the loss cone with the average kinetic energy they receive when ejected—at the expense of the MBHB's orbital energy—through the slingshot mechanism. Denoting by $\mathcal{F}_{\rm lc}(E,t)$ the time-dependent flux into the loss cone and by $\langle \Delta E(E)\rangle$ the mean kinetic energy imparted to stars which are scattered off by the binary, the hardening rate is given by (Yu 2002)

$$\frac{d}{dt}\left(\frac{1}{a}\right) = \frac{2m_*}{GM_{12}\mu_r}\int_0^{+\infty} dE \langle \Delta E(E)\rangle \mathcal{F}_{\rm lc}(E,t), \qquad (2)$$

where $E = GM_{12}/r + \Phi_*(r) - 1/2\ v^2$, and $\Phi_*(r)$ is the gravitational potential due to the stars. The mean kinetic energy $\langle \Delta E(E)\rangle$ is given by

$$\langle \Delta E(E)\rangle \sim \langle C\rangle \frac{G\mu_r}{a}, \qquad (3)$$

where $\langle C\rangle \approx 1.25$ is a dimensionless quantity obtained from three-body scattering experiments (Quinlan 1996). Therefore, the hardening rate $s(t)$ can be rewritten as

$$s(t) \equiv \frac{d}{dt}\left(\frac{1}{a}\right) \approx \frac{2m_*\langle C\rangle}{M_{12}a}\int_0^{+\infty} dE \mathcal{F}_{\rm lc}(E,t). \qquad (4)$$

The time evolution of the flux $\mathcal{F}_{\rm lc}(E,t)$ depends on the symmetries of the gravitational potential—and on the orbit families it supports. In principle, $\mathcal{F}_{\rm lc}(E,t)$ in the spherical case can be obtained from Fokker–Planck calculations that take into account the diffusion of stars in phase space (Merritt et al. 2007; Preto & Amaro-Seoane 2010). Here we derive simple scaling relations which are useful in interpreting the *N*-body results. For each energy E, $\mathcal{F}_{\rm lc}(E,t) \propto n(E,t)/T_{\rm rlx}(E,t)$, where $n(E,t)$ is the number of stars of energy E per unit energy and $T_{\rm rlx}(E,t) \propto \sigma^3/\rho m_*$ is the two-body relaxation time (Spitzer 1987, p. 191). The flux of stars into the loss cone is expected to peak around r_h (Perets & Alexander 2008), so we evaluate quantities there. Hence, $\sigma_h^2 \sim G(M(<r_h) + M_{12})/r_h \sim 3GM_{12}/r_h \propto M_{12}^{1/2}$—where $r_h \propto M_\bullet^{1/2}$ follows from the $M_\bullet$–σ relation (Ferrarese & Ford 2005). Then, $\sigma_h^3 \propto M_{12}^{3/4}$ obtains. On the other hand, for a fixed galaxy mass, we have $m_* \propto 1/N$ and therefore $T_{\rm rlx} \propto M_{12}^{3/4} N/\rho$. Since in our *N*-body models, $\rho(r)$ and $n(E,t)$ are unchanged and only σ changes as M_{12} is varied, we find that the hardening rate scales with M_{12} and N as $s \propto M_{12}^{-7/4} N^{-1}$. The case of a triaxial nucleus is different: J for each star is not conserved, thus stars may precess into the loss cone on a timescale $T_{\rm pr} \ll T_{\rm rlx}$ (Yu 2002; Merritt & Poon 2004); $T_{\rm pr}$ depends only on the global gravitational potential. In this case, the mass flux into the loss cone $m_*\mathcal{F}_{\rm lc}(E,t) \propto m_* n(E,t)/T_{pr}(E,t)$, and also $s(t)$, will be independent of N.

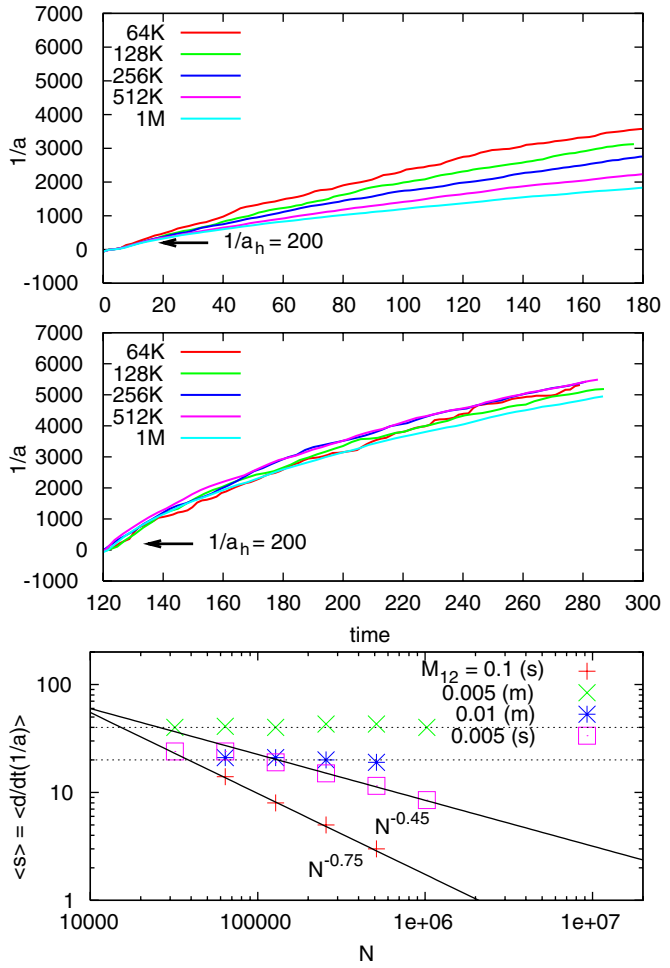

Figure 1. Binary hardening. Upper panel: in a spherical nucleus, $s(t)$ decreases with N. Middle panel: in a merging nucleus, $s(t)$ is N-independent. Lower panel: hardening rates as a function of N for different M_{12}. $\langle s\rangle$ of the $M_{12} = 0.1$ binary has been multiplied by 100. Labels "s" for spherical and "m" for merger.

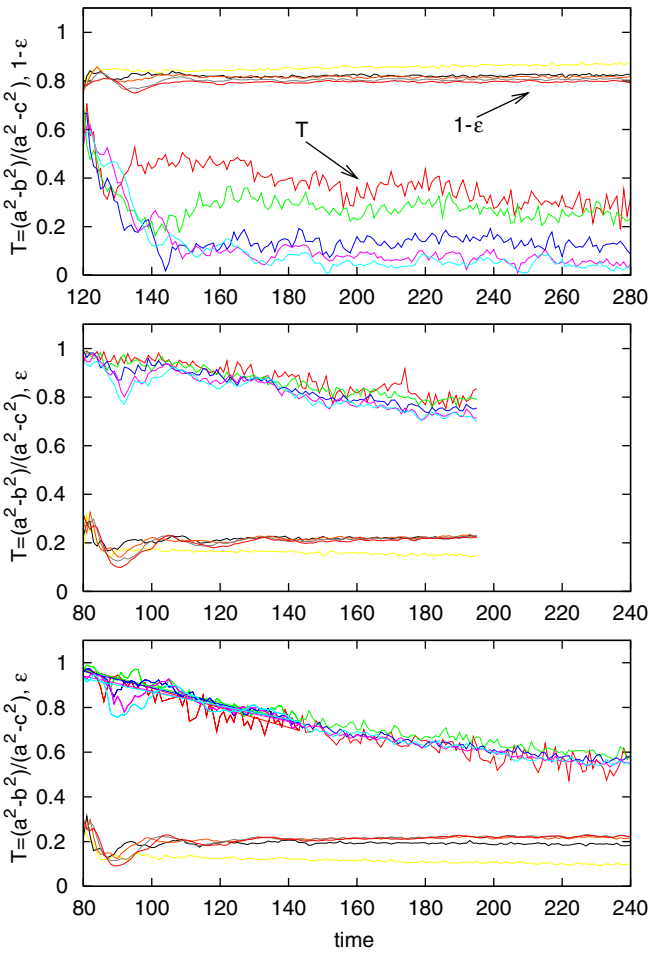

Figure 2. Triaxiality T and mass flattening of merging nuclei. Shown are binaries of $M_{12} = 0.005$, $L/L_c = 0.6$ (upper panel); $M_{12} = 0.01$, 0.02, $L/L_c = 0.14$ (middle and lower panels). T and ϵ are measured in five shells between $r = 0$ and $r = 2.5$, of width $\Delta r = 0.5$. Triaxiality decreases over time, faster for heavy binaries. Mass flattening is constant.

In Figure 1, we see that $s(t)$ is N-dependent in a spherical nucleus, while it is N-independent in the merging one. In the former case, $s(t) \propto N^{-\alpha}$, with $\alpha = 0.45$ and 0.75 for binaries of $M_{12} = 0.005$ and 0.1, respectively. These results can be interpreted as follows. In the empty loss cone limit ($\alpha = 1$), the stars repopulate the loss cone at a rate $\propto T_{\rm rlx}^{-1}$ much lower than that with which they are ejected by the binary, which is $\propto T_{\rm dyn}^{-1}$. In the full loss cone limit ($\alpha = 0$), stars enter the loss cone at a rate which is similar to the rate at which they are ejected by the binary. A measure for the loss cone refilling rate is given by (Lightman & Shapiro 1977)

$$q(E) \equiv \left(\frac{\delta J}{J_{\rm lc}}\right)^2, \qquad (5)$$

where δJ is the mean change in J, per orbital period, of a star on a low-J. In the limit $q(E) \ll 1$, the loss cone is said to be empty, while $q(E) \gg 1$ in the full loss cone limit. For a given nucleus, and for $r > r_h$, we expect δJ to be independent of M_{12}. As a result, the weaker dependence of $\langle s\rangle$ on N for lighter binaries, placed in a spherical nucleus, follows from $q \propto M_{12}^{-1/2}$; at the same E, $q(E)$ of the $M_{12} = 0.005$ binary is $\sim$4.5 larger than that of the $M_{12} = 0.1$ one. We would need to use a larger N for the lighter binaries, $\langle s\rangle \propto N^{-0.45}$, to reach the empty loss cone limit $\langle s\rangle \propto N^{-1}$; the heavier binary, $\langle s\rangle \propto N^{-0.75}$, almost reaches this limit. The dependence of $\langle s\rangle$ on M_{12} is more straightforward to interpret. For the spherical case, the lighter binary is expected to harden at a rate $\sim 20^{7/4}$ higher than the heavier, which is indeed the case. In the merger case, $m_* \mathcal{F}_{\rm lc}(E)$ is N-independent and therefore $\langle s\rangle \propto M_{12}^{-1}$. Since the mass ratio between the binaries is 2, $\langle s\rangle$ also differs by a factor of two.

We measure the triaxiality of the nucleus with $T = (a^2 - b^2)/(a^2 - c^2)$. Figure 2 depicts the evolution of T and of the flattening $\epsilon = 1 - c/a$ for several mass shells of merging nuclei. The value of T, immediately after the merger, depends on the initial L/L_c. In the case of a near-radial merger, $L/L_c = 0.14$, the remnant is prolate and evolves over time toward an oblate spheroidal shape; for $L/L_c = 0.6$ the remnant is an oblate spheroid from the very beginning. The triaxiality decreases over time, and the rate at which it changes is faster the larger M_{12} is. The triaxiality remains significant, in the inner mass shells, until the binary reaches the relativistic phase in all models with the smallest (and more realistic) values of M_{12}, and also in most of the other cases. The flattening $\epsilon \sim 0.2$ is constant throughout in all cases, so the asymptotic shape of the merger is that of an oblate spheroid. We conclude that the rather mild triaxiality created during the merger supports a family of centrophilic orbits that keep the loss cone full ($\alpha = 0$) at all times until the binary reaches relativistic separations $\sim a_{\rm GW}$.

4. ECCENTRICITY EVOLUTION AND TIMESCALES FOR COALESCENCE

The hardening rate, due to the slingshot ejection of stars, is in our N-body simulations independent of the binary's orbital elements, while that due to GWs is strongly dependent on them: $d/dt(1/a)_{GW} \sim |\dot{a}/a^2|_{\rm GW} \propto a^{-5}(1-e^2)^{-7/2}$ (Peters 1964). As a result, the binary's coalescence time $T_{\rm coal}$ depends strongly on its eccentricity. In Paper I, we did follow this evolution self-consistently with N-body simulations of rotating King models. Since such calculations are extremely CPU-intensive, we estimate the full evolution using a semi-analytic approach (Quinlan 1996). The advantage is that we can calibrate the average hardening rate $\langle s \rangle$ with our N-body simulations—which would remain a free parameter otherwise—and thus make quantitative predictions on both the coalescence times and the long-term eccentricity evolution.

The evolution of the MBHB orbital elements, including orbital energy lost to GWs, is given by

$$\frac{d}{dt}\left(\frac{1}{a}\right) = \frac{d}{dt}\left(\frac{1}{a}\right)_{st} + \frac{d}{dt}\left(\frac{1}{a}\right)_{\rm GW}$$
$$\frac{de}{dt} = \left(\frac{de}{dt}\right)_{st} + \left(\frac{de}{dt}\right)_{\rm GW}. \quad (6)$$

The GW terms are from Peters (1964). The eccentricity evolution, driven by the stars, is obtained from scattering experiments:

$$\left(\frac{de}{dt}\right)_{st} = K(e)\, a\, \langle s \rangle, \quad (7)$$

where $K(e) = e(1-e^2)^{k_0}(k_1 + k_2 e)$ and the constants are taken from Quinlan (1996). In order to assess the quality of the fits to the N-body results, Figure 3 compares the N-body evolution of the binary with that obtained from the semi-analytic model. We take as initial conditions for the integration of Equations (6) an instant of time in the early hard binary phase. Given the differences between our N-body models and the assumptions embodied by the semi-analytic description the agreement is quite remarkable.

We then include the GW terms due to radiation reaction to compute $T_{\rm coal}$. To scale our models to binaries with $M_{12} = 10^6\, M_\odot$ and $M_{12} = 10^8\, M_\odot$, we adopt the most recent observational values for the mass normalization of the Galactic center, $M(<1\ {\rm pc}) = 10^6\, M_\odot$ (Schödel et al. 2009) and use the $M_\bullet$–σ relation to extrapolate to different MBH masses. The results are shown in the upper panel of Figure 4. We see that coalescence times range between $T_{\rm coal} \sim 10^7$ yr and $\sim$ few $\times\, 10^8$ yr. These are not longer than the mean time between successive major mergers. In contrast, for a spherical nucleus, $T_{\rm coal} \sim$ few $\times$ Gyr for $M_{12} = 10^6\, M_\odot$, while binaries with $\gtrsim 10^8\, M_\odot$ would stall (M. Preto et al. 2011, in preparation).

Our coalescence times are significantly shorter than those reported by Khan et al. (2011). The approximations they make in computing $T_{\rm coal}$ lead to an overestimation by factors of $\sim$10 for $e \gtrsim 0.75$, and $\sim$4 for $e \sim 0.5$. Contrary to what is observed with post–Newtonian (PN) MBHBs (Berentzen et al. 2009; Preto et al. 2009), their $T_{\rm coal}$ is dominated by the GW inspiral phase. Another difference is that we scale our models using the $M_\bullet$–σ relation, while they do not. We are currently pursuing N-body simulations including PN terms to the binary's motion in order to resolve this discrepancy.

We also follow the long-term evolution of the eccentricity. In the N-body runs, the binaries become bound with high eccentricities (up to $e \sim 0.95$) on average—in agreement with previous works (Berentzen et al. 2009; Preto et al. 2009). Since *LISA* will be sensitive to the inspiral signal of $10^6\, M_\odot$ binaries, it is important for data analysis purposes to estimate whether they will enter the band with non-negligible eccentricity ($e \gtrsim 10^{-4}$; Porter & Sesana 2010; Shapiro Key & Cornish 2010). The middle panel of Figure 4 displays the distribution of eccentricities at $a = 100 R_{\rm Schw}$[8]—most binaries will not be fully circularized by then. We expect therefore that the eccentricity in the *LISA* band will be non-negligible. Finally, the lower panel of Figure 4 depicts the eccentricity distribution at $f_{\rm GW} = 2 f_{\rm orb} = 10^{-8}$ Hz for the PTA band. We see that eccentricities are quite high—peaking at $e \sim 0.6$. The results presented here concerning coalescence times and eccentricity growth corroborate recent three-body scattering studies—which had to treat the average hardening rate $\langle s \rangle$ as a free parameter (Sesana 2010).

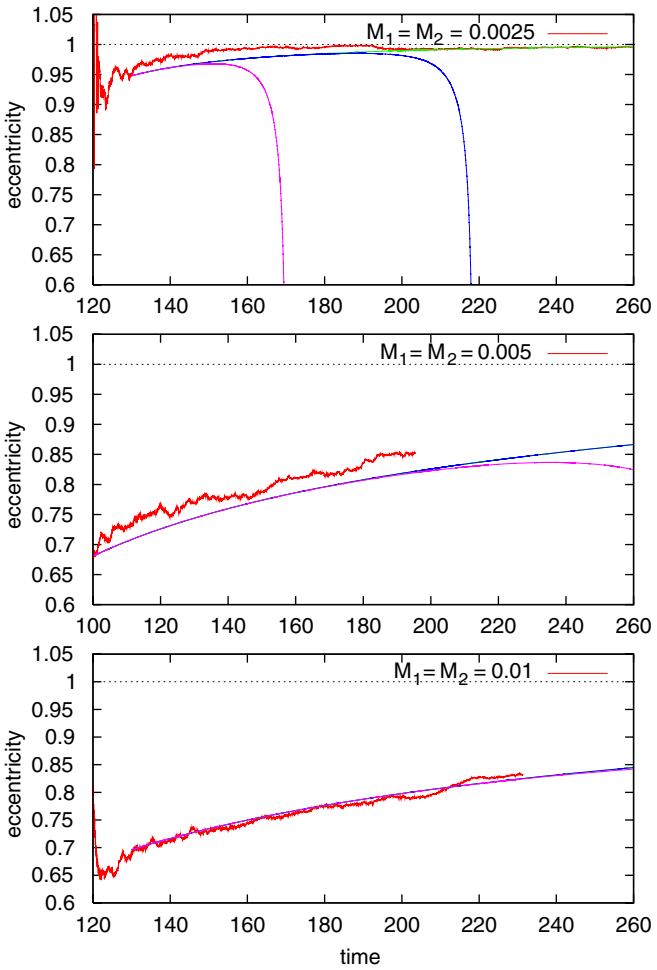

Figure 3. Eccentricity evolution. Red and green lines represent N-body and semi-analytic evolution without radiation reaction. Blue and magenta lines correspond to semi-analytic solution, including radiation reaction, for $M_{12} = 10^6\, M_\odot$ and $M_{12} = 10^8\, M_\odot$, respectively.

5. SUMMARY

With our results, we are moving closer toward a consistent solution to the Final Parsec Problem, and of providing dynamical substantiation to the cosmological scenario where prompt

[8] $R_{\rm Schw} = 2GM_{12}/c^2$, where c is the speed of light, is the Schwarzschild radius.

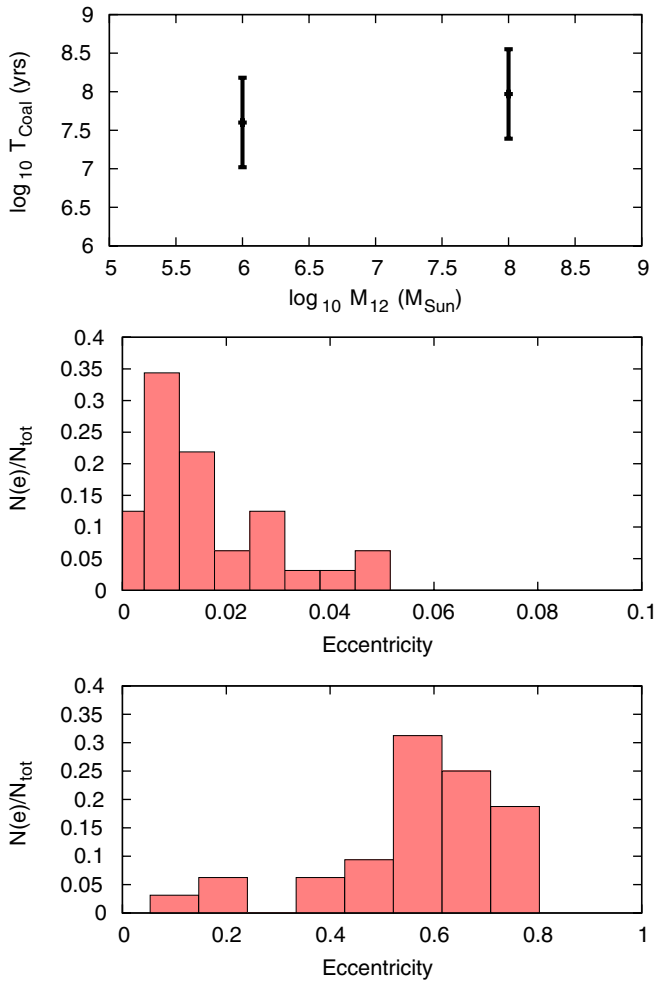

Figure 4. Upper panel: range of coalescence time for binaries with $M_{12} = 10^6\,M_\odot$ and $10^8\,M_\odot$. Middle panel: distribution of eccentricities, for $M_{12} = 10^6\,M_\odot$, at $a_{\rm bin} = 100R_{\rm Schw}$. Lower panel: distribution of eccentricities, for $M_{12} = 10^8\,M_\odot$, when $f_{\rm orb} = 2\,f_{\rm GW} = 10^{-8}$ Hz for PTAs.

coalescences are assumed during the course of galaxy evolution (Sesana et al. 2007; Volonteri 2010). Our results suggest that the formation of eccentric binaries, followed by quick orbital decay, could result from the expected development of global non-axisymmetries in galaxies after they merge. Unequal-mass mergers have similar $\langle s \rangle$ (M. Preto et al. 2011, in preparation; P. Berczik et al. 2011, in preparation). As a result, if there is a bottleneck to coalescence, it results from the long timescale associated to the formation of a bound pair in an unequal-mass galaxy merger—especially if $q \lesssim 0.1$ (Callegari et al. 2011).

Our gas-poor merger models show only rather mild departures from axisymmetry and a small amount of rotation; stronger departures from axisymmetry—to be expected from higher amount of rotation—and the presence of gas will likely reinforce our conclusions. It seems, therefore, probable that prompt coalescences result from mergers of irregular galaxies expected to be common at high redshift. Based on our prompt MBHB coalescence results, we expect that *LISA* will see $\sim$10 to few $\times$ 10^2 events per year depending on the MBH seed model (Sesana et al. 2009; Volonteri 2010). These conclusions need to be qualified in one respect: the effect of gas could be rather subtle. Several effects may result from the presence of gas: (1) circularization of the unbound MBH trajectories may lead to the formation of circular binaries (Dotti et al. 2007), however, bar instabilities may affect this conclusion (Begelman & Shlosman 2009); (2) gas torques may increase the (bound) binary's eccentricity; and (3) the outer, cooler regions of a circumbinary disk may fragment, producing a fresh supply of (mostly) bound stars to interact with the binary (Cuadra et al. 2009).

Finally, even though GWs circularize the MBHBs during the late relativistic phase of inspiral, they are likely to have some residual ($e \gtrsim 0.001$–0.01) eccentricity when entering the *LISA* band and a broad distribution ($0.4 \lesssim e \lesssim 0.8$) in the PTA band.

We thank the anonymous referee for thoughtful comments. M.P. acknowledges support by DLR (Deutsches Zentrum für Luft- und Raumfahrt). P.B. acknowledges support by NAS Ukraine under the Main Astronomical Observatory GPU/GRID computing cluster project and Cosmomicrophysics program. We acknowledge support by the Chinese Academy of Sciences Visiting Professorship for Senior International Scientists, grant number 2009S1-5 (The Silk Road Project; R.S. and P.B.). The special supercomputer Laohu at the High Performance Computing Center at National Astronomical Observatories, funded by Ministry of Finance under the grant ZDYZ2008-2, has been used. Simulations were also performed on the GRACE supercomputer (grants I/80 041-043 and I/84 678-680 of the Volkswagen Foundation, and 823.219-439/30 and /36 of the Ministry of Science, Research and the Arts of Baden-Württemberg). We thank the DEISA Consortium (http://www.deisa.eu), co-funded through EU FP6 projects RI-508830 and RI-031513, for support within the DEISA Extreme Computing Initiative. The Kolob cluster is funded by the excellence funds of the University of Heidelberg in the Frontier scheme.

REFERENCES

Aarseth, S. 2003, Gravitational N-Body Simulations (Cambridge: Cambridge Univ. Press)
Armitage, P., & Natarajan, P. 2005, ApJ, 634, 921
Begelman, M. C., Blandford, R. D., & Rees, M. J. 1980, Nature, 287, 307
Begelman, M. C., & Shlosman, I. 2009, ApJ, 702, 5
Berczik, P., Merritt, D., & Spurzem, R. 2005, ApJ, 633, 680
Berczik, P., Merritt, D., Spurzem, R., & Bischoff, H. P. 2006, ApJ, 642, 21
Berentzen, I., Preto, M., Berczik, P., Merritt, D., & Spurzem, R. 2009, ApJ, 695, 455 (Paper I)
Callegari, S., Kazantzidis, S., Mayer, L., Colpi, M., Bellovary, J. M., Quinn, T., & Wadsley, J. 2011, ApJ, 729, 85
Colpi, M., & Dotti, M. 2009, in Invited Review to appear on Advanced Science Letters (ASL), Special Issue on Computational Astrophysics, ed. L. Mayer, arXiv:0906.4339
Cuadra, J., Armitage, P., Alexander, R., & Begelman, M. 2009, MNRAS, 393, 1423
Dehnen, W. 1993, MNRAS, 265, 250
Dotti, M., Colpi, M., Haardt, F., & Mayer, L. 2007, MNRAS, 379, 956
Ferrarese, L., & Ford, H. 2005, Space Sci. Rev., 116, 523
Harfst, S., Gualandris, A., Merritt, D., Spurzem, R., Portegies Zwart, S., & Berczik, P. 2007, New Astron., 12, 357
Khan, F., Just, A., & Merritt, D. 2011, ApJ, in press (arXiv:1103.0272)
Khochfar, S., & Burkert, A. 2006, A&A, 445, 403
Lightman, A. P., & Shapiro, S. L. 1977, ApJ, 211, 244
Merritt, D., Mikkola, S., & Szell, A. 2007, ApJ, 671, 53
Merritt, D., & Poon, M. Y. 2004, ApJ, 606, 788
Milosavljević, M., & Merritt, D. 2003, ApJ, 596, 860
Perets, H., & Alexander, T. 2008, ApJ, 677, 146
Peters, P. C. 1964, Phys. Rev., 136, 1224
Porter, E., & Sesana, A. 2010, arXiv:1005.5296
Preto, M., & Amaro-Seoane, P. 2010, ApJ, 708, 42
Preto, M., Berentzen, I., Berczik, P., Merritt, D., & Spurzem, R. 2009, J. Phys. Conf. Ser., 154, 012049
Quinlan, G. D. 1996, New Astron., 1, 35

Quinlan, G. D., & Hernquist, L. 1997, New Astron., 2, 533
Schödel, R., Merritt, D., & Eckart, A. 2009, A&A, 502, 91
Sesana, A. 2010, ApJ, 719, 851
Sesana, A., Volonteri, M., & Haardt, F. 2007, MNRAS, 377, 1711
Sesana, A., Volonteri, M., & Haardt, F. 2009, Class. Quantum Grav., 26, 4033
Shapiro Key, J., & Cornish, N. 2010, arXiv:1006.3759
Spitzer, L. 1987, Dynamical Evolution of Globular Clusters (Princeton, NJ: Princeton Univ. Press)
Tremaine, S., Richstone, D. O., Byun, Y.-I., Dressler, A., Faber, S. M., Grillmair, C., Kormendy, J., & Lauer, T. R. 1994, AJ, 107, 634
Volonteri, M. 2010, A&AR, 18, 279
Yu, Q. 2002, MNRAS, 331, 935